

USP7 V517F mutation as a mechanism of inhibitor resistance

Received: 12 August 2024

Accepted: 7 February 2025

Published online: 14 March 2025



Yu-Ling Miao^{1,4}, Fengying Fan^{2,3,4}, Yong-Jun Cheng^{1,4}, Li Jia^{1,3},
Shan-Shan Song^{1,3}, Xia-Juan Huan^{1,3}, Xu-Bin Bao^{1,3}, Jian Ding^{1,3},
Xuekui Yu^{2,3} ✉ & Jin-Xue He^{1,3} ✉

Anticipating and addressing resistance is essential for maximizing the potential of an oncology target and effectively addressing clinical needs. In this study, we aimed to proactively outline the resistance mechanisms of USP7 inhibitors. We discovered a key treatment-emergent heterozygous mutation (V517F) in USP7 in the binding pocket of compounds as the primary cause of resistance to the USP7 inhibitor USP7-797. Our structural analysis, supported by AlphaFold2 predictions, indicates that the V517F mutation altered the conformation of the compound binding pocket, causing steric hindrance and reducing the affinity between USP7 and its inhibitors. Consistent with these predictions, the affinity between V517F mutant and USP7 inhibitors was found to reduce significantly. Conversely, substitutions at position V517 with smaller side chains, such as V517G, V517A, and V517I, do not significantly impact binding affinity. In contrast, replacement with the bulkier side chain V517Y leads to reduced binding affinity and diminished inhibitor efficacy. Furthermore, the engineered cell lines harboring the V517F mutation exhibited substantial resistance to USP7 inhibition. These data provide rationales for patient selection and the development of next-generation USP7 inhibitors designed to overcome treatment-emergent mutations.

Deubiquitinating enzymes are essential for maintaining protein homeostasis by cleaving ubiquitin chains from substrate proteins, thereby regulating critical cellular functions including DNA repair, cell cycle, and apoptosis¹. Among these enzymes, ubiquitin-specific protease 7 (USP7) stands out for its significant role, as its abnormal expression is frequently observed in malignant tumors and is associated with a poor prognosis^{2,3}. Specifically, USP7 overexpression has been shown to enhance the stability of E3 ligase murine double minute 2 (MDM2) while promoting the degradation of p53, leading to dysregulation of the MDM2-p53 pathway in tumorigenesis^{4,5}. Therefore, USP7 has served as a promising target for cancer therapy in terms of prognosis and drug development.

USP7 exhibits a modular domain architecture, consisting of an N-terminal TRAF domain (residues 54–208), a catalytic domain (residues 209–560), five ubiquitin-like (UBL) domains (residues 561–1083), and a C-terminal regulatory domain (residues 1084–1102)⁶. The catalytic domain of USP7 is characterized by a structure resembling an open hand with fingers, palm, and thumb subdomains, a feature conserved across all USP domains^{6,7}. Notably, significant structural changes are observed in the active site catalytic triad residues (Cysteine 223, Histidine 464, Aspartic acid 481) upon ubiquitin binding, facilitating the close proximity of these residues for efficient ubiquitin catalysis^{8–10}. USP7 has the ability to remove monoubiquitin molecules, as well as K48- and K63-linked polyubiquitin chains, from substrate

¹State Key Laboratory of Drug Research, Cancer Research Center, Shanghai Institute of Materia Medica, Chinese Academy of Sciences, 501 Haik Road, Shanghai 201203, China. ²State Key Laboratory of Drug Research, Cryo-Electron Microscopy Research Center, Shanghai Institute of Materia Medica, Chinese Academy of Sciences, 501 Haik Road, Shanghai 201203, China. ³University of Chinese Academy of Sciences, No.19A Yuquan Road, Beijing 100049, China.

⁴These authors contributed equally: Yu-Ling Miao, Fengying Fan, Yong-Jun Cheng. ✉ e-mail: xkyu@simm.ac.cn; jinxue_he@simm.ac.cn

proteins^{7,11}. Notably, USP7 has been shown to deubiquitinate and stabilize both MDM2 and p53, potentially leading to the promotion of p53 proteasomal degradation and disruption of the MDM2-p53 pathway^{4,5,12}. Several additional USP7 substrates, primarily associated with tumorigenesis, have been identified, including MDM4, MCM-BP, N-Myc, Rad18, DNMT1, UHRF, and RNF169, among others^{7,8,13}.

Over the past decade, there has been a significant focus on the development of potent and selective USP7 inhibitors (USP7i)¹⁴. Although clinical trials of USP7i have not been conducted yet, numerous compounds have demonstrated efficacy in inhibiting cancer cell growth both in vitro and in animal xenograft models^{15–21}. Small molecules that target the catalytic cleft of USP7 and form a covalent adduct with the active site Cys223 have been identified as irreversible inhibitors of USP7^{6,8,22,23}. The most representative compounds include P5091, P22077, P50429, HBX41108, HBX19818, and HBX28258^{6–8,22}. Given that all DUBs possess at least one ubiquitin binding site, the lack of potency and selectivity were significant issues faced by the irreversible USP7i⁶. By utilizing structure-based design techniques and drawing inspiration from known hits in the patent literature, various research groups have successfully developed XL188, FT671, USP7-797, YCH2823, and GNE-6640 as non-covalent active-site inhibitors with nanomolar potency and a high level of selectivity relative to other DUBs^{6–8,18,22}. They all inhibit ubiquitin binding through steric hindrance by either binding in near the catalytic cleft (e.g., XL188, FT671, and USP7-797) or outside the catalytic cleft (GNE-6640) within the USP7 catalytic domain^{6,7}. Structural analysis revealed that FT671, a derivative of 4-hydroxypiperidine, extends towards the finger subdomain of USP7 via a p-fluorophenyl group and lies 4.7 Å from the thiol group of Cys223^{18,22}. Despite being of a different chemical class, the thienopyridine derivative USP7-797 contains a unique pharmacophore and binds to a similar pocket as FT671^{21,22}. Furthermore, the 2-amino-4-ethylpyridin derivative GEN-6640 has been shown to non-covalently target USP7, with 12 Å distant from the catalytic Cys223, sterically hindering ubiquitin binding^{7,11,22}. Collectively, these compounds exhibit a consistent binding mode and establish similar interactions with the inactive conformation of USP7^{6–8,22}.

Research on USP7i has predominantly focused on their effectiveness in suppressing tumor growth. Recent preclinical investigations have demonstrated the antitumor effects of USP7i in various solid tumors and hematologic malignancies^{15–21}. It is noteworthy that USP7i effectively suppress tumor growth in both *TP53* wild-type and mutant cells, suggesting that USP7 inhibition can impede tumor growth through mechanisms that are reliant on and independent of p53^{15,18,20,24}. Moreover, USP7 inhibition has exhibited the capacity to induce apoptosis in multiple myeloma (MM) cells and overcome resistance to bortezomib²⁵. Furthermore, these inhibitors have been shown to sensitize tumors to a variety of other inhibitors, including PARP, PLK1, and HDAC inhibitors^{26–28}. These findings underscore the potential therapeutic value of USP7i across a wide range of preclinical cancer models.

It is widely recognized that USP7 inhibition plays a crucial role in regulating cancer cell proliferation through various mechanisms, including the stabilization of the p53–p21 axis and the degradation of other substrates like Rad18, DNMT1 and UHRF1^{15,18,24}. Our previous research has shown that the lack of p53 or p21 confers a notable resistance to USP7i, highlighting the importance of the p53 signaling pathway in determining the effectiveness of these inhibitors¹⁸. Conversely, DNMT and Rad18 are not likely to have a significant impact on the efficacy of USP7i¹⁸. A previous study has proposed that the ER stress-PERK-HSF1 axis may be involved in mediating chemoresistance to USP7i²⁹. Nevertheless, there remains a scarcity of information on the mechanisms of resistance to USP7i.

Understanding the underlying molecular mechanisms of acquired resistance to USP7i treatment is essential for monitoring, preventing, and overcoming drug resistance. Specifically, we observed the emergence of a heterozygous mutation in Exon 14 of the USP7 catalytic domain in cellular

models subjected to selection pressure with the USP7 inhibitor USP7-797. Our findings indicate that the mutation diminishes the efficacy of USP7i, and we have successfully constructed such a model system using engineered cell lines that exclusively express the mutant form of USP7.

Results

Establishment of USP7i-resistant cells with CHP-212 cells

USP7i have been shown to significantly reduce the growth of *MYCN*-amplified neuroblastoma cells, positioning USP7 as a promising therapeutic target in *MYCN*-driven neuroblastoma^{20,30}. In prior research, we found that the CHP-212 cell line, characterized by *MYCN* amplification and wild-type *TP53*, demonstrates significant sensitivity to USP7i treatment¹⁸. Additionally, treatment of CHP-212 cells with USP7i induces a concentration-dependent modulation of USP7 downstream signaling pathways^{18,31}. USP7-797 is a highly potent USP7 inhibitor with optimized cellular inhibition and oral bioavailability²¹. To investigate potential mechanisms of resistance to USP7 inhibition, we developed USP7-797-resistant variants of the CHP-212 cellular model. Notably, the CHP-212 cells maintain wild-type *TP53*, *MYCN* amplification, and wild-type status for USP7, p21, DNMT1, Rad18, and other members of the USP family members. The continuous administration of drug treatment to CHP-212 cells according to the protocol outlined in Fig. 1a resulted in the development of USP7-797-resistant variants (known as CHP-212-R_{mix}), along with the successful generation of six resistant monoclonal sublines (designated as R1–6; Fig. 1a). In order to differentiate between CHP-212 cells and the resistant sublines, the term “parental” cells were used in subsequent research.

The resistant sublines exhibited significant resistance to USP7-797, with a sensitivity reduction of 10–13 fold compared to the parental cells (Fig. 1b). Despite belonging to different chemotypes, FT671 and USP7-797 both bind to a similar pocket. As anticipated, resistant cells also exhibit a strong resistance phenotype for FT671, with IC₅₀ values 83–213 fold higher than those of parental cells (Fig. 1b). All six subclones (R1–R6) and the R_{mix} cell lines exhibited comparable resistance to FT671 and USP7-797. Consequently, we selected the R2, R3, and R6 subclones for further investigation due to their relatively faster growth rates. Previous research has indicated that both USP7-797 and FT671 bind in close proximity to the catalytic cleft, while GNE-6640 binds outside of this region, yet all three compounds inhibit ubiquitin binding through steric hindrance^{7,22}. Notably, resistant variants show only a 1.76-fold increase in resistance to GNE-6640 (Fig. 1c). These findings imply that resistant cells may significantly impact the effectiveness of USP7-797 and FT671, while having minimal impact on GNE-6640. Furthermore, the resistant cells maintained sensitivity to other chemotherapeutic agents (Adriamycin, Taxol, VCR), bortezomib, the NAE inhibitor MLN4924, and the USP1 inhibitor KSQ4279 (Fig. 1d), indicating that the resistance mechanism is not universally shared among different agents.

Acquired resistance leads to reduced G1-arrest and apoptosis in response to USP7-797

USP7 inhibition induces substantial apoptosis accompanied by G1 arrest in CHP-212 cells^{15,18}. Subsequently, an investigation was conducted to assess alterations in cell-cycle distribution and apoptosis within the resistant cells. As illustrated in Fig. 2a, the resistant cells exhibited G1 arrest even in the absence of USP7i treatments. Specifically, the percentage of parental cells in the G1 phase was 57.59%, while the R_{MIX} cells in the G1 phase reached 67.90%. However, the cell-cycle distribution of resistant variants treated with USP7-797 and FT671 was not profoundly altered (Fig. 2a), consistent with their insensitivity to USP7 inhibition. Significantly, our observations indicated that USP7 inhibition resulted in decreased apoptosis in all tested resistant variants compared to the parental cells under identical conditions (Fig. 2b, c). In line with this, USP7-797 and FT671 treatments demonstrated reduced activation of apoptosis-related proteins, including

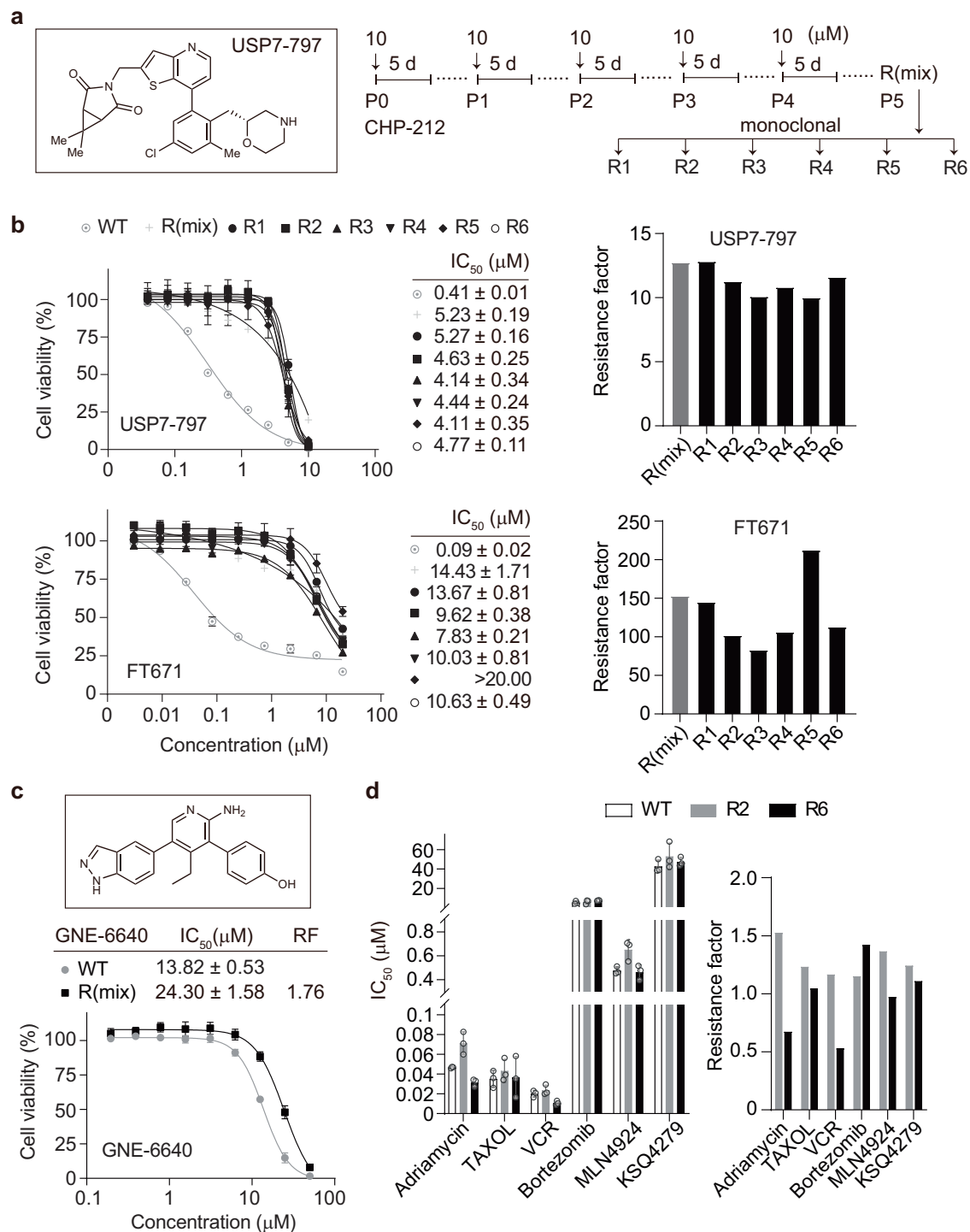


Fig. 1 | Generation of USP7i-resistant cells derived from CHP-212 cells.

a Schematic representation of the generation of USP7-797-resistant variants. CHP-212 cells were exposed to 10 μM USP7-797 for 5 days, refreshing with drug-free media, and repeating for 5 cycles. Six drug-resistant monoclonal cells (R1-R6) were selected.

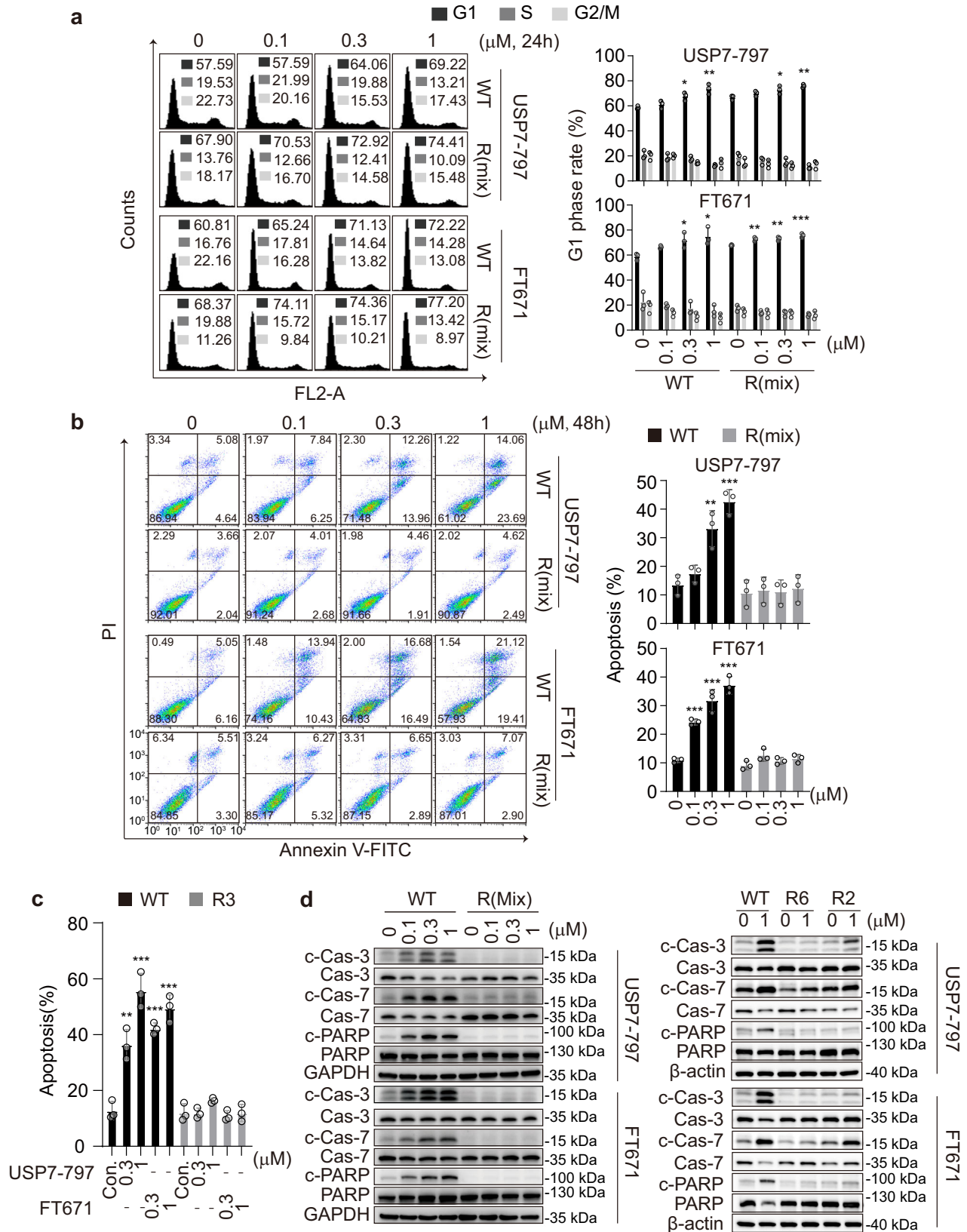
b Dose-response curves of USP7i USP7-797 and FT671 in parental and resistant cells following a 5-day exposure. Left panel, the IC₅₀ values of USP7-797 and FT671 were determined using SRB assays. Data are presented as mean ± SD (*n* = 3 technical replicates; 3 independent experiments). Right panel, the resistance factor (RF) was

calculated by comparing the average IC₅₀ value of the resistant cells to that of the parental cells. **c** The chemical structure and dose-response curves of another USP7i GNE-6640 in the parental and resistant cells. Cells were treated with GNE-6640 for 5 days, and cell viability was assessed using SRB assays. Data are presented as mean ± SD (*n* = 3 technical replicates; 3 independent experiments). **d** The IC₅₀ values of MLN4924, KSQ4279, Adriamycin, Bortezomib, TAXOL, and VCR in parental and resistant cells were determined using SRB assays following 3 days exposure. Data are presented as mean ± SD (*n* = 3 technical replicates; 3 independent experiments).

c-caspase-3, c-caspase-7, and c-PARP, in the resistant variants relative to the parent cells (Fig. 2d). These findings suggest that resistant cells exhibit resistance not only to cell cycle arrest but also to apoptotic induction by the tested USP7i.

V517F mutation in USP7 catalytic domain confer resistance

In order to investigate the potential role of alterations in the USP7 pathway in conferring resistance to USP7i, two resistant clones (R2 and R3) were subjected to analysis for genetic mutations in USP7,



substrate-related proteins, and other members of USP family. Through whole-exome sequencing (WES), it was determined that there were no treatment-emergent DNA mutations in *MDM2*, *TP53*, *CDKN1A* (p21), *RAD18*, *DNMT1*, *UHRF1*, or other USP family members such as *USP10*, *USP12*, and *USP39*. However, a heterozygous mutation in Exon 14 of *USP7* with c.G2170>T was identified in the resistant variants (Table 1).

Of note, an intronic mutation in *USP12* was found in CHP-212 parental cells, which persisted in the resistant clones. Concordance between Sanger sequencing and WES results was observed in all six CHP-212 resistant clones, revealing a mutation in Exon 14 with c.G2170>T that led to the V517F mutation form of *USP7* (*USP7_V517F*; Supplementary Table 1). These findings indicate that in vitro-derived cell lines resistant

Fig. 2 | Resistant cells demonstrate changes in cell cycle progression and apoptosis in response to USP7i. **a** Cell cycle distribution of parental and resistant cells was analyzed after treatment with USP7i for 24 h using flow cytometry. The percentage of cells in different phases of the cell cycle was determined and reported as mean \pm SD ($n = 3$ technical replicates; 3 independent experiments). **b, c** Apoptosis induced by USP7-797 or FT671 in the parental and resistant cells. Cells were exposed to different concentrations of USPi for 48 h, followed by stained with Annexin V-PI. The percentage of apoptotic cells was determined and reported

as mean \pm SD ($n = 3$ technical replicates; 3 independent experiments). **d** Protein levels of caspase family proteins and cleaved PARP1 were assessed via Western blotting. Cells were treated with USP7-797 or FT671 for 48 h and subsequently subjected to Western blotting. These experiments were repeated three times, with representative images provided. The one-way ANOVA was performed for data in (a–c). * $P < 0.05$; ** $P < 0.01$; *** $P < 0.001$, $P < 0.05$ was considered to be statistically significant. The exact P values were provided in the Source Data file.

Table 1 | Mutational status of USP7, MDM2, TP53, CDKN1A, RAD18, DNMT1, UHRF1, and other USP family members^a

Genes sequenced		CHP-212 Parental ^b	R2	R3
USP7	Sanger	WT	V517F	V517F
	Exome Sequencing	WT	V517F	V517F
MDM2		WT	WT	WT
TP53		WT	WT	WT
CDKN1A		WT	WT	WT
RAD18		WT	WT	WT
DNMT1		WT	WT	WT
UHRF1		WT	WT	WT
USP12		Intronic	Intronic	Intronic
USP10		WT	Intronic	WT
USP39		WT	WT	Copy number+8

^aOnly USP family members with detected mutations were showed in this table.

^bMutations in CHP-212 parental cells were verified in the catalog of somatic mutation in cancer (http://cancer.sanger.ac.uk/cell_lines) database, and the exome sequencing result of CHP-212 parental cells was set as the reference to that of treatment-induced resistant clones R2 and R3.

to USP7-797 has a specific mutation in the *USP7* gene, potentially contributing to their resistance. Despite having a mutant *TP53* gene, human pancreatic cancer Capan-1 cells are sensitive to USP7-797-induced cytotoxicity, with an IC_{50} value of 170 nM (Supplementary Fig. 1b). By exposing Capan-1 cells to high concentrations of USP7-797 ($\geq IC_{90}$ concentrations), resistant Capan-1 R_{mix} cell lines were established (Supplementary Fig. 1a), showing IC_{50} values of $>2 \mu M$ and $>10 \mu M$ for USP7-797 and FT671, respectively (Supplementary Fig. 1b). Nine resistant clones were isolated, but none of them showed treatment-emergent mutations in *USP7* and related genes through Sanger sequencing (Supplementary Table 1). This indicates that other resistance mechanisms may be present in these variants.

There were no substantial changes detected in the mRNA and protein levels of *USP7* (Fig. 3a). Further analysis of two resistant clones (R2 and R6) showed reduced inhibition of the *USP7* pathway with USP7-797 and FT671 treatment, as evidenced by decreased accumulation of p53 and p21, as well as degradation of substrates Rad18, DNMT1, and UHRF1 (Fig. 3b). The mutation at Valine 517 seems to be a prevalent occurrence, as nearly all detected mutations are located at this residue (Table S1 and Fig. 3c). To investigate the biochemical implications of mutations in this region, a recombinant enzyme expressing the V517F catalytic domain (CD; USP7_V517F^{CD}) was produced and validated using Coomassie Brilliant Blue fast staining (Fig. 3d, left panel). The V517F mutant enzyme displayed comparable catalytic activity to the wild-type enzyme, suggesting that the ubiquitin affinity was largely unaffected by the V517F mutation (Fig. 3d, middle and right panel). To assess the inhibitory efficacy of USP7-797 and FT671 on wild-type and mutant enzymes, a fluorogenic Ub-AMC assay was conducted with a concentration of 50 nM USP7^{CD} or USP7_V517F^{CD}. Notably, USP7-797 and FT671 failed to inhibit V517F at concentrations up to 0.5 μM or 1 μM , respectively (Fig. 3e). Furthermore, the V517F mutant exhibited approximately 2247- and 2341-fold lower susceptibility to USP7-797 and FT671, respectively, compared to the wild-type

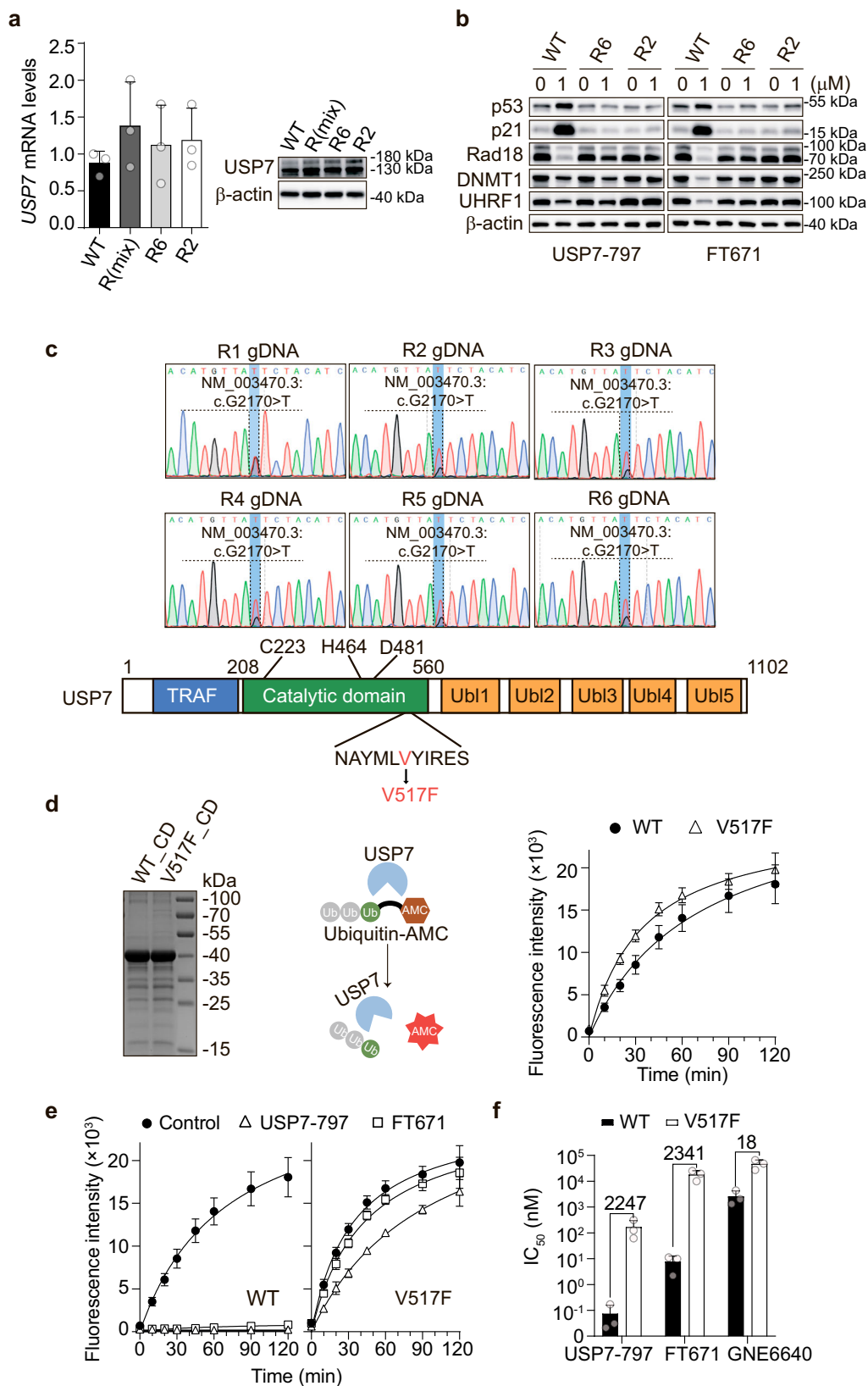
enzyme. In contrast, GNE-6640 demonstrated only an 18-fold increase in IC_{50} values for enzymatic activity inhibition in the V517F mutant compared to the wild-type enzyme (Fig. 3f and Supplementary Fig. 2a–c). Taken together, these data suggest that the V517F mutation may impact the interaction between USP7-797 and *USP7*, but does not weaken its affinity for ubiquitin. Thus, we hypothesize that the *USP7* mutation is localized to a specific region of the enzyme, proximal to the catalytic cleft, rather than within the ubiquitin binding cleft.

V517F mutation leads to weakened compound affinity

We evaluated the binding affinities of USP7_V517F to FT671 and USP7-797 utilizing isothermal titration calorimetry (ITC). As compared to the control groups, USP7_V517F exhibited a 67-fold and 57-fold decreased binding affinity to FT671 and USP7-797, respectively (Fig. 4a). To investigate how the V517F mutation affects the binding affinity of *USP7* with the small molecules, we employed AlphaFold2³² to predict the atomic model of the USP7_V517F catalytic domain (AF_USP7_V517F^{CD}, residues 206–565). The generated model shows the sidechain conformation of Y514 residue, a conserved amino acid involved in inhibitor binding^{15,21,33}, exhibited significant difference between the wild-type and the V517F mutant. While the Y514 sidechain of the wild-type USP7^{10,15,21} located outside of the inhibitor binding pocket, the counterpart of the mutant points into the binding pocket, presumably clashing with the inhibitor in that pocket (Fig. 4b; Supplementary Fig. 3; Supplementary Fig. 4a, b). Interestingly, several members of the *USP* family, including *USP4*, *USP8*, *USP9X*, *USP12*, *USP15*, and *USP34*, have been reported to be resistant to FT671¹⁵. Through structural comparison, we found that all these members^{34–39} consistently contain a phenylalanine (F) at the position equivalent to USP7 V517 (Fig. 4c). Like that of the Y514 in the USP7_V517F mutant, the sidechains of the equivalent tyrosine from the aforementioned members are also located within the inhibitor binding pocket (Fig. 4b, c). It is likely that the V517F mutation may induce sidechain conformational changes of its nearby residues due to steric hindrance, which ultimately affects the sidechain conformation of Y514, leading to reduced inhibitor binding capabilities (Fig. 4b; Supplementary Fig. 4a, b). To validate this, we constructed a series of *USP7* mutants with residue 517 bearing various sidechain in size. While the affinity of USP7_V517Y^{CD} with FT671 decreases significantly as that of the USP7_V517F^{CD}, the affinities of USP7_V517G^{CD}/V517A^{CD}/V517I^{CD} with FT671 remain essentially unchanged as compared to that of the wild-type *USP7* (Fig. 4d; Supplementary Fig. 4c). In line with this, only the V517Y mutant exhibited a significantly decreased efficiency in enzyme activity inhibition by the inhibitor (Fig. 3e; Supplementary Fig. 2a–c, Supplementary Fig. 4d).

Cells bearing V517F mutation show resistance to USP7i

As previously stated, a V517F heterozygous mutation in *USP7* has been identified, with cells retaining one wild-type copy of the gene. To definitively establish the role of this *USP7* mutation in driving resistance, it is imperative to generate engineered cell lines that exclusively express the mutant form of the enzyme. Therefore, the V517F mutation was introduced into CHP-212 cells utilizing the CRISPR/Cas9 technology. Specifically, the mutation site was deliberately integrated into the *USP7* locus through precise modification guided by sgRNA, with the aid of a donor template for strategic design (Fig. 5a, left panel). Sanger sequencing analysis of the mutant region identified homozygous CHP-



212.V517F.KI#1 and heterozygous CHP-212.V517F.KI#2 monoclonal cell lines with the knock-in mutation of V517F (Fig. 5a, right panel).

The introduction of the knock-in V517F mutation into USP7 resulted in a substantial decrease in sensitivity of USP7-797 and FT671, with sensitivity reductions ranging from 15–16 fold and 88–106 fold, respectively (Fig. 5b, left panel). Subsequent investigation of the USP7

pathway, including its impact on p53 and p21 accumulation, as well as apoptosis induction, was undertaken. Western blot analysis revealed significantly decreased levels of p53, p21, c-caspase-3, and cleave-PARP1 upon USP7i treatments in the knock-in cells compared to wild-type cells (Fig. 5b, right panel), suggesting a gain-of-function effect as expected. Given the critical role of USP7 in the MDM2-p53-p21

Fig. 3 | Resistant clones contain a heterozygous mutation in USP7. **a** The mRNA and protein levels of USP7 were assessed in parental and resistant cells using quantitative RT-PCR and Western blotting. The mRNA level are presented as mean \pm SD ($n = 3$), and blot is representative of three independent experiments. **b** Representative western blot of three experiments showing the levels of p53, p21, Rad18, DNMT1, and UHRF1 in parental and V517F mutant cells after treatment with USP7i for 24 h. **c** Schematic representation of location of USP7 mutations detected in resistant clones. Sanger sequencing confirmed the presence of the heterozygous NM_003470.3:c.G2170>T (V517F) mutation in all six resistant clones. **d** The enzyme activity of wild-type (WT) and V517F mutant was assessed by measuring the

cleavage activity of the AMC fluorophore from ubiquitin-AMC. Left panel: the catalytic domains of both the wild-type USP7 (WT_CD) and the V517F mutation (V517F_CD) were confirmed through Coomassie Brilliant Blue fast staining. Right panel: the fluorescence intensity was calculated as the mean \pm SD ($n = 3$ technical replicates; 3 independent experiments). **e** The inhibition of WT or V517F mutant by USP7-797 or FT671 was assessed to determine the enzyme activity inhibition. Data shown are the mean \pm SD ($n = 3$ technical replicates; 3 independent experiments). **f** The IC_{50} values of USP7-797, FT671, and GNE6640 in WT and V517F mutants were determined. Data are presented as mean \pm SD ($n = 3$ technical replicates; 3 independent experiments).

pathway, USP7i have shown cytotoxic effects on a subset of *TP53* wild-type tumor cells¹⁷. Our previous research indicated that *TP53* wild-type prostatic cancer LNCaP cells are highly sensitive to USP7i treatment^{18,31}. To further confirm the impact of the V517F mutation on USP7i sensitivity, the same mutant gene cassette was introduced into LNCaP cells, producing V517F.KI cells. Similarly, LNCaP.V517F.KI cells displayed increased resistance to FT671, with sensitivity reductions ranging from 121- to 146-fold (Fig. 5c, upper panel). These cells also exhibited a diminished response to USP7 pathway inhibition, as evidenced by significantly decreased levels of p21 and Rad18 (Fig. 5c, lower panel).

Previous research has demonstrated that USP7i effectively impede tumor growth through mechanisms that are both p53-dependent and p53-independent^{20,21}. In a subset of *TP53*-mutant cell lines, such as the pancreatic cancer Capan-1 cells harboring the *TP53* p.A159V mutation, USP7 inhibition has been shown to decrease cell viability^{18,20}. The transfection of full-length V517F mutant cDNA into Capan-1 cells (referred to as Capan-1.V517F.OE) significantly reduced their sensitivity to USP7-797 and FT671, compared to Capan-1 wild-type overexpressed (WT.OE) cells. This resulted in 6-fold and 48-fold higher IC_{50} values, respectively (Fig. 5d, upper panel). Additionally, Capan-1.V517F.OE cells displayed a decreased response to the USP7 pathway inhibition compared to the wild-type overexpressed cells (Fig. 5d, lower panel), suggesting a gain-of-function effect in *TP53* mutant cells. Furthermore, the overexpression of V517F in *TP53* wild-type CHP-212 and LNCaP cells led to a 5–18 fold and 29–40 fold increase in resistance to USP7i compared to their wild-type overexpressed cells (Fig. 5e). These findings collectively indicate that cell lines engineered with the V517F mutant exhibit resistance to USP7i, regardless of their *TP53* status.

Discussion

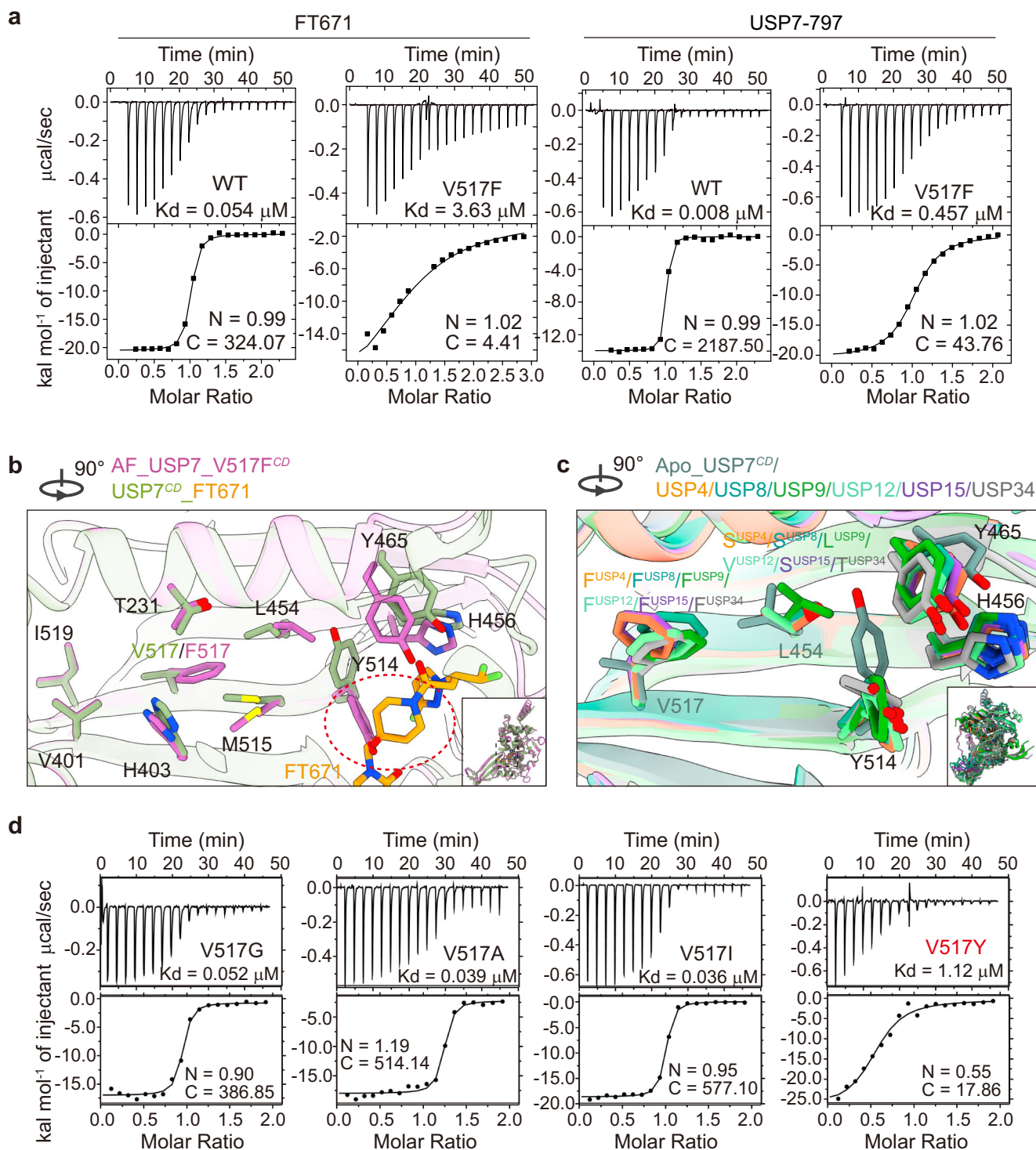
This study aimed to explore the potential resistance mechanisms to the USP7 inhibitor USP7-797 in preclinical cancer models. Our findings indicate that human tumor cell lines can acquire resistance to USP7-797 due to a coding sequence mutation in Exon 14 of *USP7* gene resulting in the V517F mutation. Structural analysis supported that the V517F mutation within the compound binding pocket of USP7 catalytic domain led to localized steric hindrance, significantly decreasing the affinity between USP7 and FT671 as well as USP7-797. The development of a V517F mutant model system using genetically modified cell lines has been successfully accomplished, confirming the mutant's resistance to USP7i. These results propose a potential strategy for the advancement of second-generation USP7i capable of surmounting resistance mechanisms.

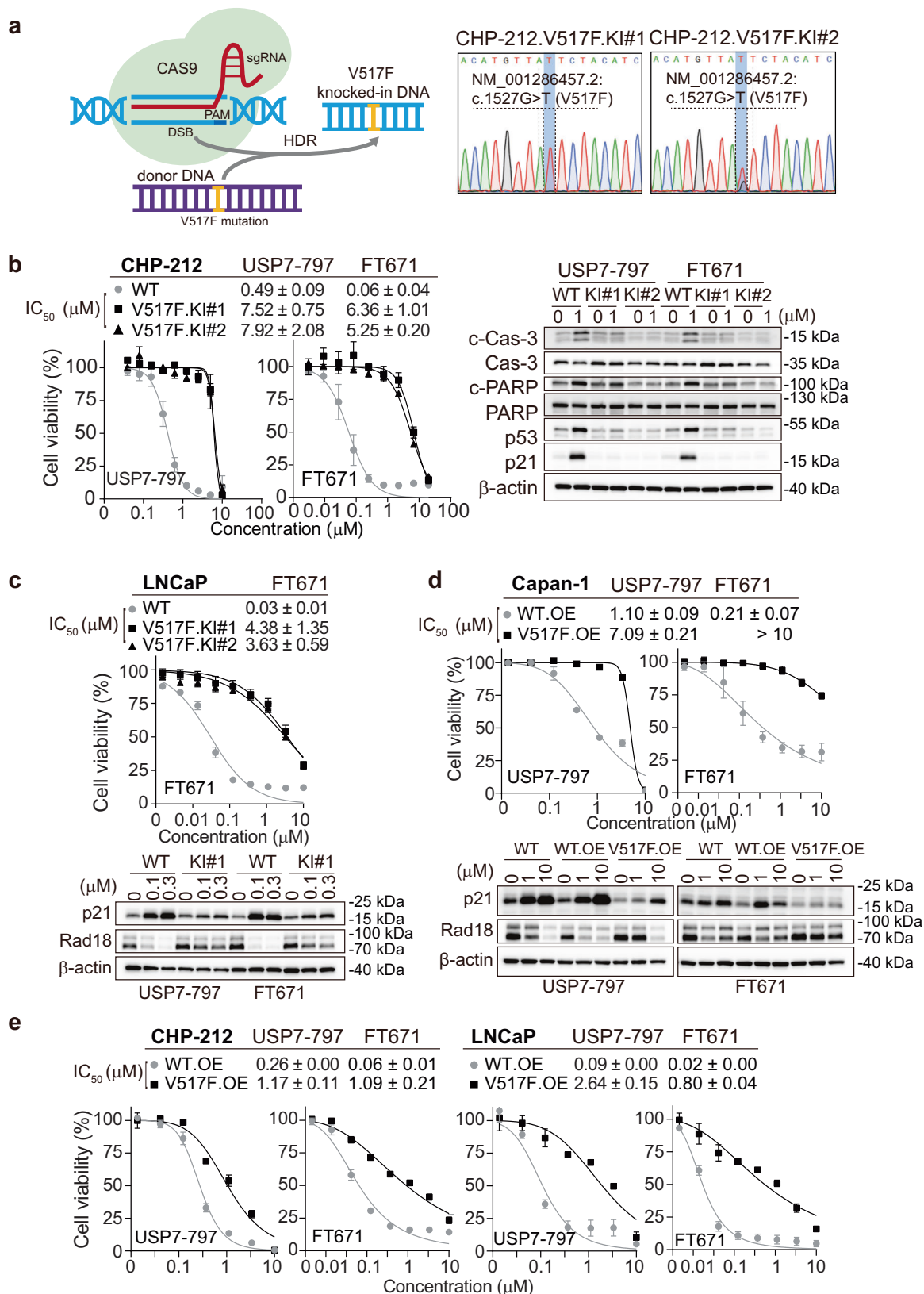
The majority of existing inhibitors focus on the catalytic domain of USP7, particularly the catalytic Cysteine 223 site^{6–8,22}. It is of interest to investigate the possibility of treatment-emergent resistance arising from USP7 inhibition. The resistant cell lines were obtained through prolonged exposure (5 days for 5 cycles) to high concentrations of USP7-797. These cell lines were subsequently isolated as clonal populations, demonstrating resistance to USP7-797, FT671, and GNE-6640, while retaining sensitivity to other chemotherapeutic agents such as Adriamycin, Taxol, VCR, bortezomib, MLN4924, and KSQ-4279. The presence of mutation in USP7 suggests that the resistance mechanism

is attributed to mutation in the target enzyme. Our findings also suggest the possibility of alternative resistance mechanisms to USP7-797, as evidenced by resistance observed in Capan-1/R cell lines lacking USP7 mutations.

This study identified a treatment-emergent mutation in USP7 located in the compound binding pocket at Valine 517, with a prevalence of approximately 100%, indicating a potential hotspot. The V517F mutant exhibited significantly reduced compound binding and inhibition, yet maintained comparable ubiquitin and ubiquitin-AFC activity. Our findings suggest that the V517F mutation plays a significant role in cross-resistance to non-covalent USP7i. Interestingly, another non-covalent FT671 with a distinct chemical structure but a common binding site²² has shown cross-resistance in USP7-797-resistant cell lines. Our findings further suggest that the V517F mutation in USP7 does not alter the overall structure of the catalytic domain. Using AlphaFold2, we created an atomic model of USP7_V517F^{CD} with the F517 located on a β -sheet within the domain, affecting the conformation of nearby residues. It seems that steric hindrance causes residue L454 to deflect, leading to a deflection in residue Y514. Specifically, Y514 is important in the FT671 binding pocket, and its altered position affects FT671 binding. Therefore, we proposed that V517F alters the binding of FT671 by changing the pocket conformation, causing a clash between Y514 and FT671 in the structures of AF_USP7_V517F^{CD} and USP7^{CD}_FT671 (Fig. 4b and Supplementary Fig. 3). Indeed, the affinity between USP7_V517F and FT671 is significantly lower than that of the wild-type USP7 and FT671. Consistent with this finding, reduced pathway inhibition and apoptosis were observed in cells treated with both USP7-797 and FT671. Notably, mutations of V517 to amino acids with smaller side chains, such as V517G, V517A, and V517I, do not significantly affect the binding affinity of the inhibitor. In contrast, mutations that introduce larger side chain, such as V517Y, result in a reduced binding affinity that is comparable to that observed with V517F (Fig. 4d). Furthermore, the inhibitor's efficacy in inhibiting enzyme activity diminishes as the side chain is replaced with bulkier residues, such as phenylalanine or tyrosine (Fig. 3e; Supplementary Fig. 4d). Amino acid substitutions have been identified as a common mechanism of resistance to cancer drugs, including tyrosine kinase inhibitors (TKIs)⁴⁰, and NAE inhibitors⁴¹. These observations have influenced treatment approaches, such as using a second-generation USP7i that can target enzymes with specific amino acid substitutions in relapsed tumors. This strategy may be advantageous in addressing resistance mechanisms involving USP7 amino acid substitutions in clinical settings in future.

A crucial approach for definitively demonstrating that mutations in USP7 drive resistance involves the creation of an engineered cell line that exclusively expresses the mutant form of the enzyme, rather than the wild-type variant. Through the utilization of CRISPR/Cas9 technology and overexpression plasmids, we have successfully generated such model systems. Specifically, the cell lines CHP-212, LNCaP, and Capan-1, which harbor the V517F.KI and V517F.OE in the context of different p53 genetic background, exhibited notable resistance to USP7-797 and FT671. The introduction of the V517F mutation into these cell lines led to the development of both heterozygous and





homozygous V517F mutant clonal cells, all of which exhibited resistance to USP7i. This suggests that the V517F mutation contributes to resistance in a dominant-negative manner. A search of single-nucleotide polymorphism database (COSMIC) did not identify the existence of the V517F mutation in human populations, suggesting that these mutations may be acquired during the selection process. As

demonstrated by the results of multiple sequence alignment conducted by Ye et al., the residue F is notably conserved at the equivalent 517 positions across various members of the USP family, in contrast to the V517 residue observed in USP7³³. However, the essential components of the compound binding pocket, specifically Y514 and Y465, display a high degree of conservation³³. This pattern of conservation

Fig. 5 | Cell lines containing the V517F knock-in mutation and overexpression demonstrate resistance to USP7i. **a** Schematic representation of generation of V517F knock-in (KI) cell lines in CHP-212 cells using CRISPR/Cas9 technology. The nucleotide sequences of the USP7 gene at the target site in the V517F KI monoclonal cells are shown in the right panel. **b, c** The CHP-212 V517F KI and LNCaP V517F KI clones exhibit resistance to USP7i and a reduction in USP7 pathway inhibition. Following treatment with the specified compounds for 5 days, cell viability was assessed using the SRB assay for CHP-212, and CCK8 assay for LNCaP cells. Western blotting analysis was conducted to assess the indicated protein levels following treatment with 1 μ M USP7-797 or FT671 for 24 h. Data shown are mean \pm SD ($n = 3$

technical replicates; 3 independent experiments). **d** Exogenous expression of V517F mutant in Capan-1 cells resulted in reduced sensitivity to USP7i. Following stable transfection with full-length USP7 WT or V517F mutant, subsequent treatment with USP7-797 for indicated days was analyzed by SRB assays or western blotting (lower panel). Data shown are mean \pm SD ($n = 3$ technical replicates; 3 independent experiments). **e** Exogenous expression of V517F mutant in CHP-212 and LNCaP cells decreased their sensitivity to USP7i. Cells were treated with USP7-797 or FT671 for 5 days and then subjected to SRB or CCK8 assays. Data shown are mean \pm SD ($n = 3$ technical replicates; 3 independent experiments).

suggests that treatment-emergent mutations are more likely to occur at V517 rather than at the conserved residues Y514 and Y465. Several members of the USP family, including USP4, USP8, USP9X, USP12, USP15, and USP34, have been documented to exhibit resistance to FT671¹⁵. Consistently, our observations indicate that all these members uniformly possess a phenylalanine (F) residue at the position analogous to USP7 V517 (Fig. 4c). Furthermore, the side chains of Y514 in these members are consistently situated within the ligand binding pocket, as observed in the USP7 V517F variant. Moreover, specific mutations in USP7 have been documented in the cBioPortal database in bladder, lung, and glioblastoma cancer samples at Exon 14 (D481H, D483N, E491K, D502E, D504N/Y_R508delinSG, and R508*/L). Continued investigation is warranted to determine the presence of pre-existing mutations, as they may serve as predictive indicators for relapse in patients receiving USP7i treatment in future.

Since V517F mutation appears to be the most common cause of resistance in our studies, it would be a promising strategy to developing a second-generation USP7i that can target the V517F mutant enzyme. Further investigation into the mechanisms of resistance to USP7i will inform ongoing clinical strategies for treating patients. This may involve combining complementary biological agents with USP7 inhibition or developing next-generation inhibitors tailored to emerging mutant USP7 enzymes in relapsed patients.

Methods

Drugs and antibodies

USP7-797 was obtained from Kerigen Therapeutics (Nangtong, China). FT671, GNE-6640, and Taxol were purchased from MedChemExpress (Monmouth Junction, NJ, USA). Adriamycin and VCR were purchased from MeilunBio (Liaoning, China). Bortezomib and MLN4924 were purchased from Selleck Chemicals (Shanghai, China). KSQ4279 was purchased from Chengdu Giant Biomedical Technology (Chengdu, China). Drugs were dissolved in dimethyl sulfoxide (DMSO), aliquoted, and stored at -20°C .

Primary antibodies were purchased from Cell Signaling Technology (Danvers, MA, USA) against the following: p21 (#2947); Rad18 (#9040); DNMT1 (#5032); UHRF1 (#12387); caspase-3 (#9662); cleaved caspase-3 (#9661); caspase-7 (#12827); cleaved caspase-7 (#8438); PARP1 (#9542). Antibody against p53 (#sc-126) was purchased from Santa Cruz Biotechnology (Dallas, TX, USA). Antibody against β -actin (60008-1Ig) was purchased from Proteintech (Hubei, China). Antibody against USP7 (ab108931) was purchased from Abcam (Cambridge, England). Antibody against GAPDH (AG019) was purchased from Beyotime Biotechnology (Shanghai, China). The secondary antibodies were purchased from Jackson ImmunoResearch Laboratories (West Grove, PA, USA).

Cell culture

Human cell lines CHP-212 (CRL-2273) and Capan-1 (HTB-79) were purchased from the American Type Culture Collection (Manassas, VA, USA). Human cell line LNCaP (SCSP-5021) was purchased from the Shanghai Institutes for Biological Sciences at the Chinese Academy of Sciences (Shanghai, China). The cells were authenticated by STR (short

tandem repeats) DNA profiling and confirmed as negative for *Mycoplasma* contamination.

CHP-212 cells and their resistant clones were maintained in a 1:1 mixture of F12 medium and MEM medium (both from Gibco), supplemented with 10% fetal bovine serum, 1% nonessential amino acids, and 1% sodium pyruvate (all from Gibco) throughout the experimental duration. LNCaP cells were cultured in RPMI-1640 medium (Gibco) with the addition of 10% fetal bovine serum (Gibco). Capan-1 cells were grown in IMDM medium (Gibco) supplemented with 10% fetal bovine serum (Gibco). The cell lines were cultured and maintained at 37°C with 5% CO_2 in a humidified environment.

Establishment of USP7i-resistant variants

To establish USP7-797-resistant cell lines, *TP53* wild-type CHP-212 cells and *TP53* mutant Capan-1 cells were plated at a density of $4\text{--}6 \times 10^5$ cells per well in 6-well plate, and were exposed to 10 μM USP7-797 (above the IC95 concentration) for a period of 5 days, followed by a recovery period in drug-free media (For CHP-212, 1:1 mixture of F12 medium and MEM medium, supplemented with 10% fetal bovine serum, 1% nonessential amino acids, and 1% sodium pyruvate; for Capan-1, IMDM medium supplemented with 10% fetal bovine serum) until cell viability was restored (P0 \rightarrow P1). This process was repeated for a total of 5 cycles (P0 \rightarrow P5). The resulting P5 CHP-212 cells were designated as CHP-212-R(mix), from which six drug-resistant single-cell clones (R1–R6) were isolated. Similarly, the P5 Capan-1 cells were designated as Capan-1-R(mix), from which nine drug-resistant single-cell clones (E1–E6, D3, D4, and D6) were selected.

Cell viability assay

Cells were plated at a density of 1000–6500 cells per well in 96-well plates before treatment with indicated drugs at varying concentrations for 3–5 d. To measure cell viability, sulforhodamine B (SRB) and CCK-8 assays were performed⁴². CHP-212 and Capan-1 cells were fixed with pre-cooled trichloroacetic acid (TCA; Sinopharm Chemical Reagent Co., Ltd.; Shanghai, China) overnight at 4°C , followed by five washes with distillation-distillation H_2O (dd H_2O). The cells were then stained with SRB (Sigma-Aldrich; St. Louis, MO, USA) for 15 min. Excess SRB was removed using 1% acetic acid solution (Sinopharm Chemical ReagentCo., Ltd; Shanghai, China), and 10 mM Tris(hydroxymethyl) aminomethane solution was added to dissolve the SRB. Absorbance was measured at 560 nm using a SpectraMax 190 Microplate Reader. The inhibition rate (%) was calculated as follows:

$$\left[1 - \left(\frac{A560_{\text{treated}}}{A560_{\text{control}}} \right) \right] \times 100\% \quad (1)$$

For LNCaP cells, 10 μl of CCK-8 (Meilunbio, Liaoning, China) was added per well to the cell culture medium at the end of compound treatment. The cells were then incubated for an additional 3–6 h before measuring the absorbance ratio using the SpectraMax 190 Microplate Reader at 450 nm, ensuring it fell within the range of 0.8–1.2.

The inhibition rate (%) was calculated as follows:

$$\left[1 - \left(\frac{A450_{\text{treated}}}{A450_{\text{control}}} \right) \right] \times 100\% \quad (2)$$

The IC₅₀ value was calculated using the Logit method.

Western blotting and Coomassie brilliant blue fast staining

The cellular level of the indicated proteins was measured using the standard Western blotting protocol. In brief, cells treated with indicated drugs were lysed using SDS lysis buffer (50 mM Tris-HCl, pH 6.8, 2% SDS, 0.05% bromophenol blue, 10% glycerin, and 100 mM DTT) and subjected to boiling for 15 min. The cell lysates were subjected to separation by SDS-PAGE on 7.5–12.5% acrylamide gels at 90 V for 25 min and 180 V for 55 min. Coomassie Brilliant Blue Fast Staining solution (#P1300; Solarbio Life Science; Beijing, China) was then utilized for Coomassie brilliant blue fast staining according to the manufacturer's instructions. For western blotting analysis, the separated proteins were transferred to a 0.45 μM nitrocellulose membrane using Trans-Blot Turbo (Bio-Rad), and subsequently blocked with TBST 5% milk for 1 h. The membranes were then incubated with primary antibodies at a dilution of 1:1000, followed by secondary anti-rabbit-HRP or anti-mouse-HRP antibodies. The signal was analyzed using a Bio-Rad ChemiDoc Imaging system.

Flow cytometry

Cell cycle distribution and apoptosis were assessed using flow cytometry¹⁸. After treatment with USP7-797, FT671 or 0.01% of DMSO for the indicated time, CHP-212 parental and resistant cells were prepared for the assessment of cell cycle distribution or apoptosis. In the case of cell cycle analysis, cells were exposed to the indicated drugs for 24 h, fixed with 70% ethanol overnight at 4 °C, treated with RNase A for 15 min, and subsequently stained with propidium iodide (Beyotime; Shanghai, China) for 30 min. For apoptosis analysis, cells were incubated with indicated drugs for 48 h, harvested, and stained with FITC Annexin V and propidium iodide following the manufacturer's protocols (Apoptosis Detection Kit I, #556547; BD Pharmingen). All data were acquired using a FACS Calibur instrument (BD Biosciences; USA) and analyzed with FlowJo V10 software. The gating strategy was depicted in Supplementary Fig. 5.

Whole-exome sequencing

The cell samples of CHP-212 and two resistant variants (CHP-212#R2 and CHP-212#R3) underwent whole-exome sequencing conducted by RIBBIO (Guangzhou, China). Briefly, genomic DNA extraction was carried out using the Megan HiPure Blood & Tissue DNA Kit (No. D3018; Magen; Guangzhou, China) following the manufacturer's protocol. Fragmented genomic DNA was then ligated to adapters for whole-exome library construction, and targeted enrichment was achieved through capture by Agilent SureSelect Human All Exon V6 + COSMIC (66 M). The captured fragments were subsequently analyzed using the Illumina HiSeq platform (Illumina, CA, USA) with paired-end sequencing. Quality assessment of sequencing reads was conducted using Fast QC, and adapter removal and read trimming were performed using Trimmomatic. Each sample should have a minimum of 12 G of clean reads and a Q30 value greater than 90%. Following this, the clean reads were aligned to the human reference genome sequence (hg19) using BWA v0.7.1.

Local realignment around insertion/deletions (InDels) was conducted using the Genome Analysis Tool kit (GATK) after removing duplicated reads with the Picard tool. Mutations were detected by comparing the bam files of parental cells and resistant clones using Mutect2/VarScan2. The predicted single nucleotide variants (SNVs) and InDels were subjected to further filtering criteria, which included: (i) ≥10 reads containing the mutation in the resistant clone file; (ii) mutations

present in >20% of the reads mapped to the mutation locus; (iii) ≥8 reads covering the mutation locus in the parental clone file; and (iv) ≤2% of reads containing the mutation in the parental clone file. Copy number alterations were identified using CONTROL-FREEC/ExomeCNV. Subsequently, the mutations were annotated using Annovar with the NCBI dbSNP and COSMIC databases, as well as sorting intolerant from tolerant (SIFT) and polymorphism phenotyping (PolyPhen) scores.

DNA sequencing

DNA isolation of resistant variants of CHP-212 and Capan-1 was carried out using a AxyPrep™ Multisource Genomic DNA Miniprep Kit (Corning), while a MolPure® Cell/Tissue DNA Kit (Yeasen) was utilized for the DNA isolation of knocked-in cells, following the manufacturer's protocols. The primers were synthesized by Sangon Biotech (Shanghai, China) as follows:

USP7-F: 5'-TTGTATGAGCGGATGCTGA-3';

USP7-R: 5'-TGCATCGAAACGCGCAAG-3'.

PCR amplifications of USP7 were conducted using optimized cycling conditions with the primers USP7-F and USP7-R, followed by sequencing of the amplified products using Sanger sequencing at BGI Genomics (Shanghai, China). Point mutations were manually confirmed by aligning sequencing data with the corresponding referencing sequence in SnapGene Version 4.3.6.

Quantitative real-time PCR (qRT-PCR)

Total RNA extraction was performed using the SteadyPure Quick RNA Extraction Kit (#AG21023; Accurate Biology; Hunan, China) in accordance with the manufacturer's instructions. cDNA was generated using HiScript III RT SuperMix (Vazyme; Jiangsu, China) for qPCR, and qRT-PCR reactions were carried out on the CFX Connect™ Real-Time System (Bio-RAD). Primers USP7-RT-F and USP7-RT-R were utilized for *USP7*, while β-actin-RT-F and β-actin-RT-R were used for *β-actin*, all of which were synthesized by Sangon Biotech (Shanghai, China) as follows:

USP7-RT-F: 5'-GTCACGATGACGACCTGTCTGT-3';

USP7-RT-R: 5'-GTAATCGCTCCACCAACTGCTG-3';

β-actin-RT-F: 5'-TCGTGCGTGACATTAAGGAG-3';

β-actin-RT-R: 5'-ATGCCAGGGTACATGGTGGT-3'.

The relative mRNA expression of USP7 was normalized from the *β-actin* transcript levels using the comparative Ct method in Bio-Rad CFX Manager 3.1.

Gene knock-in

The sgRNA and ssDNA were purchased from Genscript (Nanjing, China) as follows: USP7-sgRNA: 5'-GCTTACATGTTAGTCTACATC-3'; USP7-ssDNA: 5'-TGTCTGTTTCGACACTGCACTAATGCTTACATGTTAT TCTACATCAGAGAATCAAACTGAGTGAGTAGTGTCTACT-3'. CHP-212 and LNCaP cells were transfected utilizing the Neon™ Transfection System (MPK5000s; Invitrogen; Carlsbad, CA, USA) in accordance with the manufacturer's guidelines. Specifically, a mixture containing 22.5 μM USP7-sgRNA and 7.5 μM GenCRISPR™ Cas9 v1.2 (#Z03702; Genscript; Nanjing, China) in R buffer (Invitrogen; Carlsbad, CA, USA) was prepared to a final volume of 7 μl. Following a 10-min incubation at room temperature, 1 μg ssDNA was introduced and allowed to incubate for an additional 2 min. Subsequently, 3 × 10⁵ CHP-212 cells were added into the system. The resulting mixture was loaded into 10 μl tips and subjected to electroporation using one of two settings: Setting 1, 1400 volts, 20 ms width, and 2 pulses; Setting 2, 1700 volts, 20 ms width, and 1 pulse. In the case of LNCaP cells, 1 × 10⁶ cells were electroporated in a 100 μl tip using settings of 1250 volts, 20 ms width, and 2 pulses. Subsequently, single-cell clones were chosen, and the efficacy of gene knock-in was confirmed through Sanger sequencing.

Stable overexpression of USP7 and USP7_V517F

USP7 and USP7_V517F were stably overexpressed using pCDH-CMV-GFP-Puro vectors through lentiviral infection. Briefly, the wild-type

cDNA of human USP7 (residues 208–560; HG11681-G) was purchased from Sino Biological (Beijing, China). Amplification of the wild-type USP7 was conducted using the primers USP7-OV-F and USP7-OV-R. The V517F mutation was introduced into USP7 through a three-step PCR based site-directed mutagenesis technique⁴³, employing the wild-type cDNA of USP7 as the template and utilizing two sets of primers (USP7-OV-F with USP7-V517F-R, and USP7-V517F-F with USP7-OV-R). All primers were synthesized by Sangon Biotech (Shanghai, China) as follows:

USP7-OV-F: 5'-ACCTCCATAGAAGATTCTAGACGCGGGATATGAAC CAC-3';

USP7-OV-R: 5'-GATCGCAGATCCTTCGCGGCCGCGCCGACTAGT GATTCAGTTATG-3';

USP7-V517F-F: 5'-GCTTACATGTTATTCTACATCAGGGAATC-3';

USP7-V517F-R: 5'-GATTCCTGATGTAGAATAACATGTAAGC-3'.

Both wild-type USP7 and USP7_V517F were cloned into the XbaI/NotI restriction sites of the pCDH-CMV-MCS-EF1-CopGFP-T2A-Puro vectors (DB00013; MiaolingBio; Wuhan, China). Subsequently, lentiviruses were generated by co-transfecting HEK293T cells with psPAX2 (Addgene plasmid #12260), PMD2.G (Addgene plasmid #12259), and the recombinant pCDH-CMV-GFP-Puro plasmids. CHP-212, Capan-1, and LNCaP cells were then infected with the lentiviruses for 48 h to overexpress USP7 and USP7_V517F. The clones with overexpression were then selected using 2 µg/ml puromycin for additional 7 days, and successful gene overexpression was validated via Western blotting analysis.

Protein expression and purification

The cDNA of USP7 mutants V517G, V517A, V517I, and V517Y were purchased from GenScript (Nanjing, China). His-tagged USP7^{CD}, V517F^{CD}, V517G^{CD}, V517A^{CD}, V517I^{CD}, and V517Y^{CD} were inserted into the pET28 vector and expressed in *E. coli* BL21 (DE3). The *E. coli* was cultured in LB liquid medium supplemented with 50 mg/ml Kanamycin at 37°C until reaching an OD_{600nm} of 0.8, followed by induction with 0.5 mM IPTG at 17°C overnight. The pellet was then resuspended in lysis buffer (50 mM HEPES, 300 mM NaCl, 10 mM Imidazole, 3 mM β-Mercaptoethanol, pH 7.5) and sonicated for lysis. After centrifugation to clarify the lysate, the supernatant was applied to a Ni-NTA gravity column (Beyotime, Shanghai, China), washed with lysis buffer containing 100 mM Imidazole, and eluted with 250 mM Imidazole. The protein was concentrated using an Amicon Ultra-15 Centrifugal Filter (MerckMillipore; Germany), purified by desalting through a gravity column (Sangon Biotech; Shanghai, China), and confirmed through Western blotting and Coomassie brilliant blue fast staining.

In vitro enzyme assays

The inhibitory effects of compounds on the enzymatic activity of USP7^{CD}, V517F^{CD}, V517G^{CD}, V517A^{CD}, V517I^{CD}, and V517Y^{CD} were assessed by measuring the increase in fluorescence resulting from the cleavage of ubiquitin-7-amino-4-methylcoumarin (Ub-AMC; Bio-Techne)¹⁸. The IC₅₀ values were determined through serial dilution of USP7-797, FT671, or GNE6640, which were pre-incubated for 15 min with 3 nM of USP7^{CD} or each mutant protein in a 384-well plate containing 50 mM Tris-HCl, 0.5 mM EDTA, 5 mM DTT, 0.01% Triton, and 0.05% BSA at pH 7.6. Subsequently, 80 nM ubiquitin-AMC was added, and the reaction was carried out at 27°C. The reaction proceeded for a duration of 2 h until the addition of 200 mM acetic acid to halt the reaction, followed by the measurement of fluorescence intensity using a SynergyTM HI (Bio-Tek) equipped with a 380 nm excitation/505 nm emission optic module.

The inhibition rate (%) was calculated as follows:

$$\left[1 - \left(\frac{\text{Fluorescence Intensity}_{\text{compound}}}{\text{Fluorescence Intensity}_{\text{USP7}} - \text{Fluorescence Intensity}_{\text{blank}}} \right) \right] \times 100\% \quad (3)$$

The IC₅₀ value was calculated by the Logit method using Graphpad Prism 9.1.

In the time-dependent inhibition assay, either 0.5 µM USP7-797 or 1 µM FT671 was incubated with 50 nM USP7^{CD} or other mutant isoforms under the same reaction conditions as described above, except that fluorescence intensity was measured at the time points of 0, 10, 20, 30, 45, 60, 90, 120, and 150 min after the initiation of the reaction without the addition of acetic acid for termination.

Isothermal titration calorimetry (ITC) assays

ITC assays of USP7^{CD} and V517F^{CD} were conducted at room temperature using a MicroCal iTC200 (Malvern Panalytical), and the ITC data for V517G^{CD}, V517A^{CD}, V517I^{CD}, and V517Y^{CD} were collected using a MicroCal PEAQ-ITC (Malvern Panalytical)¹⁸. Recombinant USP7^{CD}, V517F^{CD}, V517G^{CD}, V517A^{CD}, V517I^{CD}, or V517Y^{CD} was titrated with first injection of 0.5 µL, and followed with 20 injections (2 µL per injection) at 25°C of USP7-797 or FT671. The dissociation constant (Kd) values were calculated by fitting the data set using the single-site binding model provided by MicroCal PEAQ-ITC analysis software. The experimental setups of all ITC measurements were provided in Supplementary Table 2.

Predicted model by AlphaFold2

All the predicted models are generated using AlphaFold2³² installed on local workstation. Structural comparisons are performed by using ChimeraX⁴⁴.

Statistical analyses

All statistical data were assessed via Graphpad Prism 7.0 and presented as mean ± SD without special statements. **P* < 0.05; ***P* < 0.01; ****P* < 0.001, *P* < 0.05 was considered to be statistically significant.

Reporting summary

Further information on research design is available in the Nature Portfolio Reporting Summary linked to this article.

Data availability

The structures of USP7 in complex with FT671, USP4, USP8, USP9X, USP12, USP15, USP34, USP7, and USP7 in complex with Compound 23 are taken from the Protein Data Bank under the accession codes [5NGE](#), [2Y6E](#), [2GFO](#), [5WCH](#), [5K16](#), [6GHA](#), [7W3R](#), [INB8](#), [6VN3](#).

The sequencing data generated in this study have been deposited in the NCBI SRA database under accession code [PRJNA1149296](#). All other data are available within this article, or are provided in the Supplementary Information/Source Data file. Source data are provided with this paper.

Code availability

No custom code or mathematical algorithms employed in this study, and no original code is reported.

References

- Clague, M. J., Urbé, S. & Komander, D. Breaking the chains: deubiquitylating enzyme specificity begets function. *Nat. Rev. Mol. Cell Biol.* **20**, 321–321 (2019).
- Zhao, G. Y. et al. USP7 overexpression predicts a poor prognosis in lung squamous cell carcinoma and large cell carcinoma. *Tumor Biol.* **36**, 1721–1729 (2015).
- Zhang, L., Wang, H., Tian, L. & Li, H. X. Expression of USP7 and MARCH7 is correlated with poor prognosis in epithelial ovarian cancer. *Tohoku J. Exp. Med.* **239**, 165–175 (2016).
- Li, M. Y. et al. Deubiquitination of p53 by HAUSP is an important pathway for p53 stabilization. *Nature* **416**, 648–653 (2002).
- Sheng, Y. et al. Molecular recognition of p53 and MDM2 by USP7/HAUSP. *Nat. Struct. Mol. Biol.* **13**, 285–291 (2006).

6. Wertz, I. E. & Murray, J. M. Structurally-defined deubiquitinase inhibitors provide opportunities to investigate disease mechanisms. *Drug Discov. Today* **31**, 109–123 (2019).
7. Valles, G. J., Bezsonova, I., Woodgate, R. & Ashton, N. W. USP7 is a master regulator of genome stability. *Front. Cell Dev. Biol.* <https://doi.org/10.3389/fcell.2020.00717> (2020).
8. Guo, N. J. et al. USP7 as an emerging therapeutic target: a key regulator of protein homeostasis. *Int. J. Biol. Macromol.* <https://doi.org/10.1016/j.ijbiomac.2024.130309> (2024).
9. Rougé, L. et al. Molecular understanding of USP7 substrate recognition and C-terminal activation. *Structure* **24**, 1335–1345 (2016).
10. Hu, M. et al. Crystal structure of a UBP-family deubiquitinating enzyme in isolation and in complex with ubiquitin aldehyde. *Cell* **111**, 1041–1054 (2002).
11. Kategaya, L. et al. USP7 small-molecule inhibitors interfere with ubiquitin binding. *Nature* **550**, 534–538 (2017).
12. Li, M. Y., Brooks, C. L., Kon, N. & Gu, W. A dynamic role of HAUSP in the p53-Mdm2 pathway. *Mol. Cell* **13**, 879–886 (2004).
13. Pozhidaeva, A. & Bersonova, I. USP7: structure, substrate specificity, and inhibition. *DNA Repair* **76**, 30–39 (2019).
14. Li, P., Liu, Y. & Liu, H. M. A patent review of ubiquitin-specific protease 7 (USP7) inhibitors (2014-present). *Expert Opin. Ther. Pat.* **32**, 753–767 (2022).
15. Turnbull, A. P. et al. Molecular basis of USP7 inhibition by selective small-molecule inhibitors. *Nature* **550**, 481–486 (2017).
16. Lamberto, I. et al. Structure-guided development of a potent and selective non-covalent active-site inhibitor of USP7. *Cell Chem. Biol.* **24**, 1490–1500 (2017).
17. Gavory, G. et al. Discovery and characterization of highly potent and selective allosteric USP7 inhibitors. *Nat. Chem. Biol.* **14**, 118–125 (2018).
18. Cheng, Y. J. et al. Identification of YCH2823 as a novel USP7 inhibitor for cancer therapy. *Biochem. Pharmacol.* <https://doi.org/10.1016/j.bcp.2024.116071> (2024).
19. Li, X. et al. Discovery of orally bioavailable n-benzylpiperidinol derivatives as potent and selective USP7 inhibitors with in vivo antitumor immunity activity against colon cancer. *J. Med. Chem.* **65**, 16622–16639 (2022).
20. Ohol, Y. M. et al. Novel, selective inhibitors of USP7 uncover multiple mechanisms of antitumor activity in vitro and in vivo. *Mol. Cancer Therap.* **19**, 1970–1980 (2020).
21. Leger, P. R. et al. Discovery of potent, selective, and orally bioavailable inhibitors of USP7 with in vivo antitumor activity. *J. Med. Chem.* **63**, 5398–5420 (2020).
22. Oliveira, R. I., Guedes, R. A. & Salvador, J. A. R. Highlights in USP7 inhibitors for cancer treatment. *Front. Chem.* <https://doi.org/10.3389/fchem.2022.1005727> (2022).
23. Reverdy, C. et al. Discovery of specific inhibitors of human USP7/HAUSP deubiquitinating enzyme. *Chem. Biol.* **19**, 467–477 (2012).
24. Pei, Y. et al. Discovery of a potent and selective degrader for USP7. *Angew. Chem. Int. Ed.* <https://doi.org/10.1002/anie.202204395> (2022).
25. Yao, Y. et al. Blockade of deubiquitinase USP7 overcomes bortezomib resistance by suppressing NF- κ B signaling pathway in multiple myeloma. *J. Leukoc. Biol.* **104**, 1105–1115 (2018).
26. Morra, F. et al. The combined effect of USP7 inhibitors and PARP inhibitors in hormone-sensitive and castration-resistant prostate cancer cells. *Oncotarget* **8**, 31815–31829 (2017).
27. Granieri, L. et al. Targeting the USP7/RRM2 axis drives senescence and sensitizes melanoma cells to HDAC/LSD1 inhibitors. *Cell Rep.* **40**, 111396 (2022).
28. Shin, S. B., Kim, C. H., Jang, H. R. & Yim, H. Combination of inhibitors of USP7 and PLK1 has a strong synergism against paclitaxel resistance. *Int. J. Mol. Sci.* <https://doi.org/10.3390/ijms21228629> (2020).
29. Lim, C. H. et al. ER Stress-activated HSF1 governs cancer cell resistance to USP7 inhibitor-based chemotherapy through the PERK pathway. *Int. J. Mol. Sci.* <https://doi.org/10.3390/ijms25052768> (2024).
30. Tavana, O. et al. HAUSP deubiquitinates and stabilizes N-Myc in neuroblastoma. *Nat. Med.* **22**, 1180–1186 (2016).
31. Zhuang, Z. et al. Discovery of pyrrolo[2,3-d]pyrimidin-4-one derivative YCH3124 as a potent USP7 inhibitor for cancer therapy. *Eur. J. Med. Chem.* **277**, 116752 (2024).
32. Jumper, J. et al. Highly accurate protein structure prediction with AlphaFold. *Nature* **596**, 583–589 (2021).
33. Ye, Y., Scheel, H., Hofmann, K. & Komander, D. Dissection of USP catalytic domains reveals five common insertion points. *Mol. Biosyst.* **5**, 1797–1808 (2009).
34. Clerici, M., Luna-Vargas, M. P., Faesen, A. C. & Sixma, T. K. The DUSP-Ubl domain of USP4 enhances its catalytic efficiency by promoting ubiquitin exchange. *Nat. Commun.* **5**, 5399 (2014).
35. Avvakumov, G. V. et al. Amino-terminal dimerization, NRDP1-rhodanese interaction, and inhibited catalytic domain conformation of the ubiquitin-specific protease 8 (USP8). *J. Biol. Chem.* **281**, 38061–38070 (2006).
36. Paudel, P. et al. Crystal structure and activity-based labeling reveal the mechanisms for linkage-specific substrate recognition by deubiquitinase USP9X. *Proc. Natl Acad. Sci. USA* **116**, 7288–7297 (2019).
37. Li, H. et al. Allosteric activation of ubiquitin-specific proteases by β -propeller proteins UAF1 and WDR20. *Mol. Cell* **63**, 249–260 (2016).
38. Ward, S. J. et al. The structure of the deubiquitinase USP15 reveals a misaligned catalytic triad and an open ubiquitin-binding channel. *J. Biol. Chem.* **293**, 17362–17374 (2018).
39. Xu, G. et al. Structural insights into the catalytic mechanism and ubiquitin recognition of USP34. *J. Mol. Biol.* <https://doi.org/10.1016/j.jmb.2022.167634> (2022).
40. Chen, Y. & Fu, L. Mechanisms of acquired resistance to tyrosine kinase inhibitors. *Acta Pharm. Sin. B* **1**, 197–207 (2011).
41. Milhollen, M. A. et al. Treatment-emergent mutations in NAE β confer resistance to the NEDD8-activating enzyme inhibitor MLN4924. *Cancer Cell* **21**, 388–401 (2012).
42. Wang, L. M. et al. Thioparib inhibits homologous recombination repair, activates the type I IFN response, and overcomes olaparib resistance. *Embo Mol. Med.* <https://doi.org/10.15252/emmm.202216235> (2023).
43. Andreassen, P. R., Pettersen, J. S. & Jørgensen, M. Site-directed mutagenesis for in vitro and in vivo experiments exemplified with RNA interactions in *Escherichia coli*. *J. Vis. Exp.* <https://doi.org/10.3791/58996> (2019).
44. Meng, E. C. et al. UCSF ChimeraX: tools for structure building and analysis. *Protein Sci.* **32**, e4792 (2023).

Acknowledgements

This work was supported by grants from the National Natural Science Foundation of China (82073875 to J.H.), the State Key Laboratory of Drug Research; and the National Key Research and Development Program of China (2022YFC3400500 to X.Y.). We thank the staff members of the Large-scale Protein Preparation System (<https://cstr.cn/31129.02.NFPS.LSPS>) at the National Facility for Protein Science in Shanghai (<https://cstr.cn/31129.02.NFPS>), for providing technical support and assistance in data collection and analysis.

Author contributions

J.H., X.Y., and J.D. supervised the project. J.H., X.Y., Y.M., Y.C., and F.F. designed experiments. J.H., X.Y., Y.M., and F.F. wrote the paper. Y.C., Y.M., L.J., S.S., X.H., and X.B. completed the in vitro experiments and related data analysis. F.F. completed the model prediction by

AlphaFold2. X.Y. and F.F. interpreted the result of model prediction. All authors contributed to the writing and revising of the paper.

Competing interests

The authors declare no competing interests.

Additional information

Supplementary information The online version contains supplementary material available at <https://doi.org/10.1038/s41467-025-56981-w>.

Correspondence and requests for materials should be addressed to Xuekui Yu or Jin-Xue He.

Peer review information *Nature Communications* thanks Benedikt Kessler, who co-reviewed with Hannah Jones, and the other, anonymous, reviewer(s) for their contribution to the peer review of this work. A peer review file is available.

Reprints and permissions information is available at <http://www.nature.com/reprints>

Publisher's note Springer Nature remains neutral with regard to jurisdictional claims in published maps and institutional affiliations.

Open Access This article is licensed under a Creative Commons Attribution-NonCommercial-NoDerivatives 4.0 International License, which permits any non-commercial use, sharing, distribution and reproduction in any medium or format, as long as you give appropriate credit to the original author(s) and the source, provide a link to the Creative Commons licence, and indicate if you modified the licensed material. You do not have permission under this licence to share adapted material derived from this article or parts of it. The images or other third party material in this article are included in the article's Creative Commons licence, unless indicated otherwise in a credit line to the material. If material is not included in the article's Creative Commons licence and your intended use is not permitted by statutory regulation or exceeds the permitted use, you will need to obtain permission directly from the copyright holder. To view a copy of this licence, visit <http://creativecommons.org/licenses/by-nc-nd/4.0/>.

© The Author(s) 2025